



## Influence of sources and atmospheric processes on metal solubility in PM<sub>2.5</sub> in urban Guangzhou, South China

Zhisheng Zhang <sup>a</sup>, Jun Tao <sup>b,\*</sup>, Leiming Zhang <sup>c</sup>, Bangkai Hu <sup>b</sup>, Ming Liu <sup>a</sup>, Fuli Nie <sup>a</sup>, Haitao Lu <sup>a</sup>, Laiguo Chen <sup>a</sup>, Yunfei Wu <sup>d</sup>, Duohong Chen <sup>e</sup>, Boguang Wang <sup>b</sup>, Huizheng Che <sup>f</sup>

<sup>a</sup> South China Institute of Environmental Sciences, Ministry of Ecology and Environment, Guangzhou, China

<sup>b</sup> College of Environment and Climate, Institute for Environmental and Climate Research, Jinan University, Guangzhou, China

<sup>c</sup> Air Quality Research Division, Science and Technology Branch, Environment and Climate Change Canada, Toronto, Canada

<sup>d</sup> Key Laboratory of Middle Atmosphere and Global Environment Observation, Institute of Atmospheric Physics, Chinese Academy of Sciences, Beijing, China

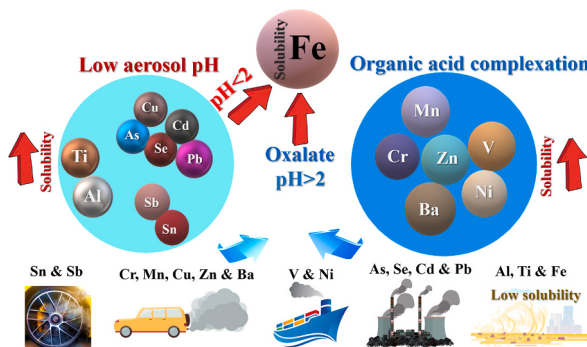
<sup>e</sup> Environmental Key Laboratory of Regional Air Quality Monitoring, Ministry of Ecology and Environment, Guangdong Ecological and Environmental Monitoring Center, Guangzhou, China

<sup>f</sup> State Key Laboratory of Severe Weather & Key Laboratory of Atmospheric Chemistry of CMA, Chinese Academy of Meteorological Sciences, Beijing, China

### HIGHLIGHTS

- Crustal metals are less soluble than those from combustion.
- Cu, As, Se, Cd, Sn, Sb, Pb, Al, and Ti solubilities increase with aerosol acidity.
- V, Cr, Mn, Ni, Zn, and Ba solubilities rise due to organic acid complexation.
- Fe solubility depends on aerosol acidity and organic acid complexation.

### GRAPHICAL ABSTRACT



### ARTICLE INFO

Editor: Hai Guo

#### Keywords:

Aerosol acidity  
Crustal sources  
Non-exhaust emissions  
Organic acid complexation  
Transition metal

### ABSTRACT

Water-soluble metals exert a significant influence on human and ecosystem health. In this study, a comprehensive investigation was undertaken to elucidate the solubilities of metals in PM<sub>2.5</sub> and potential influencing factors during the dry season of 2019–2020 in urban Guangzhou, South China. The observed average solubility was <20 % for Al, Fe, Sn, and Ti; 20–40 % for V, Cr, Sb, Pb, and Ni; 40–60 % for Ba and Cu; and 60–80 % for Zn, As, Se, Cd, and Mn. Metals (Al, Ti, and Fe) originated from crustal sources (e.g., soil dust) have much lower solubilities than those (Mn, Zn, As, Se, Cd, and Ba) from fossil fuel combustion sources (e.g., traffic emission, coal combustion), suggesting the dominant role the metal sources played on solubility. Enhanced solubilities of Cu, As, Se, Cd, Sn, Sb, and Pb were associated with aerosol acidity, while those of V, Cr, Mn, Ni, Zn, and Ba were linked to organic acid complexation. For the three crustal metals, the solubilities of Al and Ti primarily depended on aerosol acidity, whereas the solubility of Fe depended on both aerosol acidity under pH < 2 conditions and organic acid complexation under pH > 2 conditions. These findings underscore the primary influence of inherent

\* Corresponding author.

E-mail address: [taojun@jnu.edu.cn](mailto:taojun@jnu.edu.cn) (J. Tao).



properties of the metals on their solubility and reveal the varying impacts of atmospheric physicochemical processes, with changes in their solubilities being <10 % for Cd, Sn, Sb, and Pb, 10–20 % for Cu, Cr, Mn, Ni, and Ba, and 20–30 % for As, Se, and Zn.

## 1. Introduction

Metals, especially toxic ones, in particulate matter significantly negatively affect human and ecosystem health (He et al., 2023; Ito et al., 2016; Nordberg and Costa, 2021). The water-soluble fractions of these metals are especially of concern due to their migration into the environment, high levels of bioavailability, and potential to cause adverse health effects (Li et al., 2017; Reeder et al., 2006; Sørensen et al., 2005). Water-soluble metals can also potentially impact the health and reproductive abilities of marine organisms (Mahowald et al., 2018). Metals in fine particles ( $\text{PM}_{2.5}$ ) tend to exhibit higher solubility in comparison to those in coarse particles (Badami et al., 2023; Heal et al., 2005; Mamun et al., 2019; Wang et al., 2015). Additionally, atmospheric chemical processes can enhance the solubilities of water-soluble metals, especially for transition metals (e.g., Fe, Mn, Cu) (Fu et al., 2010; Li et al., 2015; Shi et al., 2020, 2015).

The solubility of metals, or the presence of water-soluble metals in metal compounds, is intricately linked to the sources of metal emissions (Badami et al., 2023; Cheng et al., 2021; Fang et al., 2015; Galon-Negru et al., 2019; Yang and Weber, 2022). For example, metallic elements derived from combustion processes, such as Zn, Cu, Pb, and As, generally have a solubility exceeding 40 %, while crustal metals from natural soil dust, such as Fe, Ti, and Al, typically have a solubility of below 20 % (Badami et al., 2023; Heal et al., 2005; Liu et al., 2022b; Manousakas et al., 2014; Qureshi et al., 2006; Wang et al., 2015; Yang et al., 2021). Additionally, Cr from vehicle emissions shares a similarly limited solubility (below 20 %) to those of crustal metals (Badami et al., 2023; Heal et al., 2005; Liu et al., 2022b; Manousakas et al., 2014; Qureshi et al., 2006). Besides the sources of the metals, aerosol acidity and complexation with water-soluble organic matter or carboxylic acid can also impact aerosol solubilities, as has been demonstrated for Fe, the most abundant metal in Earth's crust found in particulate matter, by many existing studies (Li et al., 2017; Liu et al., 2022a; Shi et al., 2020; Srivivas et al., 2014; Tao and Murphy, 2019; Winton et al., 2016; Zhu et al., 2020).

In the recent decade,  $\text{PM}_{2.5}$  pollution in the Pearl River Delta (PRD) region of South China has been decreasing, with annual average  $\text{PM}_{2.5}$  mass concentration conforming to the Stage 2 standard ( $25 \mu\text{g m}^{-3}$ ) set by the World Health Organization (WHO). Nevertheless, the presence of metals in  $\text{PM}_{2.5}$  remains notably elevated in this region (Fu et al., 2021; Wu et al., 2019; Yan et al., 2022). Remarkably, the levels of Cr(VI) and As, both recognized as carcinogens, continue to surpass the established threshold ( $1 \times 10^{-6}$ ) for adult exposure (Huang et al., 2023). In addition, strong aerosol acidity in this region may increase the solubility of metals, thereby amplifying their adverse effects on human health (Fu et al., 2015; Jia et al., 2020). To date, a comprehensive study on the solubility of metals in  $\text{PM}_{2.5}$  and its primary influencing factors is still lacking in the PRD region. To address this knowledge gap, an integrated campaign was conducted during the dry season of 2019–2020 in urban Guangzhou to synchronously measure water-soluble metals, total metals, water-soluble inorganic ions, oxalate, and water-soluble organic carbon (WSOC) in  $\text{PM}_{2.5}$  and size-segregated samples, as well as meteorological parameters. The collected data were then analyzed to reveal the solubility of water-soluble metals in  $\text{PM}_{2.5}$  and explore major influencing factors on metal solubility. The insights generated from this study are crucial for assessing the health risks associated with water-soluble metals and formulating effective strategies to mitigate metal pollution.

## 2. Methodology

### 2.1. Sampling descriptions

The sampling site was situated in the South China Institute of Environmental Science (SCIES) in urban Guangzhou ( $23^{\circ}07'N$ ,  $113^{\circ}21'E$ ) (Fig. S1). Bulk  $\text{PM}_{2.5}$  samples were concurrently collected offline using two samplers (model LVS, Comde Derenda Corp., China) with a sampling flow of  $1.0 \text{ m}^3 \text{ h}^{-1}$ . The samplers were equipped with 47 mm Whatman polytetrafluoroethylene (PTFE) membrane filters and quartz fiber filters. Additionally, size-segregated samples were obtained offline using a high-flow seven-stage air sampler, which was operated with a constant airflow of  $560 \text{ L min}^{-1}$  through each of its seven stages. The stages were equipped with cutoff points at 0.41, 0.73, 1.4, 2.1, 4.2, and  $10.2 \mu\text{m}$  (Tisch, Series 230-High Volume Cascade Impactors, US), using quartz fiber filters (Whatman QM-A).

A total of 33  $\text{PM}_{2.5}$  samples and 4 blanks were collected across two campaigns: October 22 to November 8, 2019, and December 24, 2019 to January 7, 2020. During the second campaign, 15 size-segregated samples and one blank were collected. Each sample spanned 23 h, starting at 11:00 a.m. and ending at 10:00 a.m. the following day. Further detailed information can be found in the supplementary materials.

### 2.2. Chemical analysis of offline samples

To comprehensively analyze total metals in  $\text{PM}_{2.5}$  samples, including both insoluble and soluble forms, as well as water-soluble metals, PTFE filters were employed. To elucidate the size distribution of metal solubility, two representative quartz fiber filter samples were selected: one from December 31, 2019, exhibiting relatively low particle mass concentration, and another from January 4, 2020, which had the highest particle mass concentration among all the sampling days. These samples were used to measure both the total metal mass concentration and their water-soluble fraction.

Total metals and water-soluble metals in  $\text{PM}_{2.5}$  collected on PTFE filters were extracted using a mixed acid solution of  $\text{HNO}_3\text{-HCl}$  (1:3) and ultrapure water, respectively. The concentrations of these metals were determined using an Inductively Coupled Plasma Mass Spectrometer (ICP-MS, PerkinElmer NexION 2000, USA). Sixteen metal species (Al, Ti, V, Cr, Mn, Fe, Ni, Cu, Zn, As, Se, Cd, Sn, Sb, Ba, and Pb) were analyzed in  $\text{PM}_{2.5}$  and size-segregated samples, all with concentrations exceeding 0.5 ppb (equivalent to a mass concentration of  $0.2 \text{ ng m}^{-3}$  in the atmospheric environment). Quality assurance and control (QA/QC) for ICP-MS measurements were maintained through the analysis of the certified reference standard NIST SRM-1648a. The recovery rates for most metals were within  $\pm 15$  % of the certified values, except for As ( $\pm 20$  %), and the precision for most metals was better than 5 %.

Considering the high background value of Al in size-segregated quartz fiber filters and the concentrations of Ni and V being below the detection limit, 13 metal species (Ti, Cr, Mn, Fe, Cu, Zn, As, Se, Cd, Sn, Sb, Ba, and Pb) were analyzed in size-segregated samples. Since the mass concentration of Fe in size-segregated samples significantly surpassed the background value of Fe in quartz fiber filters, the measured mass concentration of Fe was retained. The relative standard deviation for the accuracy of most metal measurements fell in the range of 5–10 %.

Additionally, carbonaceous aerosols, comprising organic carbon (OC) and elemental carbon (EC), alongside water-soluble inorganic ions, oxalate, and water-soluble organic carbon (WSOC), were examined in offline  $\text{PM}_{2.5}$  samples collected on quartz fiber filters. Further detailed

information can be found in the supplementary materials.

### 2.3. Online measurements of total metals and other parameters

Twenty-one elements (Si, S, Cl, K, Ca, Ti, V, Cr, Mn, Fe, Ni, Cu, Zn, As, Se, Cd, Sn, Sb, Ba, Pb, and Bi) were semi-continuously measured using an online X-ray fluorescence spectrometer (XRF, Cooper Environmental Services, Model Xact 625i) equipped with a PM<sub>2.5</sub> impactor inlet. Due to the low mass concentrations of most elements, the sampling interval was set to 4 h (0:00–4:00, 4:00–8:00, 8:00–12:00, 12:00–16:00, 16:00–20:00, and 20:00–00:00). Effective online concentration data of Al could not be obtained due to the significant uncertainty in the Al mass concentration measured by the online XRF spectrometer.

Additionally, precursor gases such as NH<sub>3</sub>, HCl, and HNO<sub>3</sub> were measured by an In-situ Gas and Aerosol Composition monitoring system (Model S-611, Fortelice International Co., Ltd) with an hourly temporal resolution. Meteorological parameters, including wind direction and speed, relative humidity, temperature, and precipitation, were concurrently measured by an automatic meteorological station (Vaisala Company, model MAWS201) with a 10 min temporal resolution.

### 2.4. Data analysis

To comprehend the influence of diverse metal sources on their solubility, this study initially aimed to utilize the Positive Matrix Factorization (PMF) model for the separate analysis of both total metals and their water-soluble fractions. Regrettably, the sample count for water-soluble metals derived from the filter was limited to 33, rendering it insufficient for the PMF model. Nevertheless, strong correlations emerged ( $R^2 > 0.90$ ,  $p < 0.01$ ) between offline (starting at 11:00 a.m. and ending at 10:00 a.m. the following day) and synchronous online (starting at 12:00 a.m. and ending at 12:00 a.m. the following day) total metal measurements, as well as between total metals and their water-soluble fractions (Figs. S2 and S3). Consequently, the source apportionment results of online total metal measurements were deemed to be, to some extent, representative of the source apportionment of water-soluble metals.

To align the results of total metal source apportionment based on online and offline measurements, this study exclusively considered total metals measurable in both modes. The metals measured online by the XRF spectrometer included Ti, V, Cr, Mn, Fe, Ni, Cu, Zn, As, Se, Cd, Sn, Sb, Ba, and Pb, all of which maintained concentrations above the 4-hour detection limits. In the PMF analysis, we tested different numbers of source factors and eventually chose five source factors, which produced the most coherent source profiles, notably evidenced by an  $F_{\text{peak}}$  value of -0.1.

To determine aerosol acidity (pH), this study employed the ISO-RROPIA II model, utilizing forward mode and metastable conditions to estimate aerosol liquid water content (ALWC) and H<sup>+</sup> concentration. The input parameters encompassed ambient relative humidity, ambient temperature, mass concentrations of K<sup>+</sup>, Ca<sup>2+</sup>, Mg<sup>2+</sup>, Na<sup>+</sup>, TH<sub>2</sub>SO<sub>4</sub> (substituted with observed SO<sub>4</sub><sup>2-</sup>), TNH<sub>3</sub> (comprising NH<sub>3</sub> and NH<sub>4</sub><sup>+</sup>), TCl (comprising HCl and Cl<sup>-</sup>), and TNO<sub>3</sub> (comprising HNO<sub>3</sub> and NO<sub>3</sub><sup>-</sup>).

To trace the origins of the dust storm arriving at the SCIES site, 72-h backward trajectories were calculated using the Hybrid Single-Particle Lagrangian Integrated Trajectory model. These trajectories were determined for an arrival elevation of 100 m and arrival times of 2:00, 8:00, 14:00, and 20:00 local time.

## 3. Results and discussion

### 3.1. Overview of total and water-soluble metals mass concentrations

During the observation period, the average PM<sub>2.5</sub> concentration was  $49 \pm 20 \mu\text{g m}^{-3}$ , surpassing the WHO Interim Target 1 annual standard of  $35 \mu\text{g m}^{-3}$  by 40 %. On 15 % of the sampling days, daily mass

concentration exceeded the WHO Interim Target 1 daily standard of  $75 \mu\text{g m}^{-3}$  (Table S1). The average mass concentration of total metals measured by ICP-MS was  $971 \pm 412 \text{ ng m}^{-3}$ , accounting for only 0.02 ± 0.01 of the PM<sub>2.5</sub> mass fraction (Table 1). Enrichment factors (EFs) relative to the Earth's upper crust composition can be used to assess whether these metals in PM<sub>2.5</sub> originate from crustal or anthropogenic sources. In this study, Al was chosen as the reference metal. The average composition of the Earth's crust was referenced by Hans Wedepohl (1995). The EFs of Ti, Al, Fe, Ba, and V were <10; EFs of Mn, Cr, and Ni ranged from 10 to 100; and EFs of Cu, Pb, Sn, As, Zn, Cd, Sb, and Se were >100 (Fig. S4). These results indicate that Ti, Al, Fe, Ba, and V primarily originated from crustal sources, while the other metals were significantly influenced by anthropogenic sources.

Among the total metals measured, crustal metals exhibited the highest mass concentration, with Fe leading at  $394 \pm 156 \text{ ng m}^{-3}$  (ranging from  $132$  to  $704 \text{ ng m}^{-3}$  for daily samples), followed by Al at  $290 \pm 212 \text{ ng m}^{-3}$  (ranging from  $59$  to  $864 \text{ ng m}^{-3}$ ). Among the anthropogenic metals, Zn had the highest concentration of  $154 \pm 74 \text{ ng m}^{-3}$  (ranging from  $62$  to  $398 \text{ ng m}^{-3}$ ), followed by Pb at  $29 \pm 11 \text{ ng m}^{-3}$  (ranging from  $11$  to  $63 \text{ ng m}^{-3}$ ) (Fig. 1a). The sum of the above four metals accounted for 0.89 mass fraction of the total measured metal mass concentrations (Table 1). The average concentrations of Fe and Zn from the present study were similar to the median concentrations observed in Asia ( $405 \text{ ng m}^{-3}$  for Fe and  $200 \text{ ng m}^{-3}$  for Zn), but significantly higher than those observed in North America and Europe (Mamun et al., 2019). The average concentrations of Al and Pb from the present study slightly exceeded the median concentrations observed in Europe ( $242 \text{ ng m}^{-3}$  for Al and  $22 \text{ ng m}^{-3}$  for Pb), but were significantly lower than those observed in Asia ( $423 \text{ ng m}^{-3}$  for Al and  $80 \text{ ng m}^{-3}$  for Pb) (Mamun et al., 2019).

The average mass concentration of the total measured water-soluble metals was  $267 \pm 113 \text{ ng m}^{-3}$ , accounting for  $0.29 \pm 0.07$  of the total metal mass fractions (Table 1). Among the water-soluble metals, Fe, Al, and Zn were the most abundant, though their rankings in mass concentration differed significantly from those of the total metal mass concentrations (Fig. 1b). Water-soluble Zn had the highest mass concentration at  $127 \pm 70 \text{ ng m}^{-3}$ , substantially higher than that of water-soluble Fe ( $53 \pm 19 \text{ ng m}^{-3}$ ) and Al ( $36 \pm 15 \text{ ng m}^{-3}$ ). Additionally, Mn ( $16 \pm 8.4 \text{ ng m}^{-3}$ ) ranked as the fourth most abundant water-soluble metal, surpassing Pb ( $7.6 \pm 3.2 \text{ ng m}^{-3}$ ). These four metals collectively accounted for 0.87 of the total measured water-soluble metal mass concentrations (Table 1). The mass concentration rankings of the abundant water-soluble metals (Zn, Fe, Al, Mn, and Pb) were generally consistent with findings from studies conducted in the United States, Greece, and northern Chinese cities (Badami et al., 2023; Fang et al., 2015; Liu et al., 2022b; Manousakas et al., 2014; Wang et al., 2015). However, the mass concentrations of these metals were significantly higher than those observed in the United States and Greece (Badami et al., 2023; Fang et al., 2015; Manousakas et al., 2014). Except for water-soluble Zn, the concentrations of other water-soluble metals (Fe, Al, Mn, and Pb) were generally lower than those reported for northern Chinese cities (Liu et al., 2022b; Wang et al., 2015). Notably, the mass concentrations of water-soluble metals (Zn, Fe, Al, Mn, and Pb) in this study were lower than those at a mountain site in southern China, primarily due to cloud processes during atmospheric transport that increase the solubility of these metals (Li et al., 2015).

Besides Ba ( $p = 0.003$ ), water-soluble Fe, Zn, Mn, Cu, Ba, and Cr ( $p < 0.001$ ) were at least 50 % higher on lightly polluted days ( $\text{PM}_{2.5} > 75 \mu\text{g m}^{-3}$ ) compared to on good ( $35 \mu\text{g m}^{-3} < \text{PM}_{2.5} < 75 \mu\text{g m}^{-3}$ ) and excellent ( $\text{PM}_{2.5} < 35 \mu\text{g m}^{-3}$ ) days (Fig. 1a and b, Table 1). In particular, water-soluble transition metals, particularly Cu, Mn, and Fe, significantly contributed to the oxidative potential of particulate matter (Charrier and Anastasio, 2012; Fang et al., 2016; Lyu et al., 2018). Additionally, the mass concentrations of Mn, Fe, and Cu across all particle sizes on a typical lightly polluted day (January 4, 2020) were higher than those on a typical good day (December 31, 2019) (Fig. 2).

**Table 1**Metal's total mass concentration and water-soluble portion in PM<sub>2.5</sub> under the different daily PM<sub>2.5</sub> mass levels.

Components	Average (N = 33)		PM <sub>2.5</sub> < 35 µg m <sup>-3</sup> (N = 7)		35 < PM <sub>2.5</sub> < 75 µg m <sup>-3</sup> (N = 21)		PM <sub>2.5</sub> > 75 µg m <sup>-3</sup> (N = 5)	
	Total	Water-soluble	Total	Water-soluble	Total	Water-soluble	Total	Water-soluble
Fe/ng m <sup>-3</sup>	394 ± 156	53 ± 19	268 ± 147	34 ± 13	403 ± 141	53 ± 12	532 ± 104	82 ± 14
Al/ng m <sup>-3</sup>	290 ± 212	36 ± 15	244 ± 278	27 ± 19	307 ± 216	37 ± 13	284 ± 77	43 ± 11
Zn/ng m <sup>-3</sup>	154 ± 74	127 ± 70	84 ± 16	55 ± 11	143 ± 29	121 ± 28	294 ± 77	250 ± 84
Pb/ng m <sup>-3</sup>	29 ± 11	7.6 ± 3.2	21 ± 6.6	5.3 ± 1.9	30 ± 8.6	8.0 ± 2.9	38 ± 17	8.9 ± 4.5
Mn/ng m <sup>-3</sup>	25 ± 11	16 ± 8.4	14 ± 4.4	8.0 ± 3.1	24 ± 7.7	16 ± 5.3	44 ± 7.4	31 ± 3.6
Ti/ng m <sup>-3</sup>	23 ± 13	0.9 ± 0.3	16 ± 15	0.7 ± 0.5	24 ± 13	0.9 ± 0.3	31 ± 7.1	1.1 ± 0.1
Cu/ng m <sup>-3</sup>	17 ± 11	7.9 ± 5.1	5.6 ± 2.5	2.9 ± 1.5	16 ± 6.7	7.9 ± 3.5	35 ± 12	15 ± 6.3
Ba/ng m <sup>-3</sup>	11 ± 5.8	6.3 ± 3.7	7.0 ± 3.9	3.4 ± 2.2	11 ± 4.9	6.3 ± 3.2	18 ± 6.6	11 ± 3.9
Sn/ng m <sup>-3</sup>	5.4 ± 2.3	0.6 ± 0.2	3.4 ± 1.2	0.4 ± 0.2	5.2 ± 1.5	0.6 ± 0.1	9.1 ± 2.1	0.8 ± 0.1
As/ng m <sup>-3</sup>	5.4 ± 3.8	4.0 ± 2.9	3.9 ± 2.1	2.9 ± 1.8	5.4 ± 2.8	4.2 ± 2.2	7.8 ± 7.8	4.7 ± 5.9
Sb/ng m <sup>-3</sup>	4.7 ± 2.2	1.4 ± 0.5	3.0 ± 1.2	0.9 ± 0.4	4.4 ± 1.4	1.4 ± 0.4	8.2 ± 2.5	2.0 ± 0.4
Cr/ng m <sup>-3</sup>	3.4 ± 1.8	1.0 ± 0.6	2.0 ± 0.5	0.4 ± 0.2	3.3 ± 1.5	1.0 ± 0.4	5.5 ± 2.0	1.9 ± 0.5
Se/ng m <sup>-3</sup>	3.2 ± 1.1	2.4 ± 1.0	2.1 ± 0.6	1.7 ± 0.7	3.4 ± 1.0	2.7 ± 1.0	3.5 ± 1.0	2.1 ± 0.7
Ni/ng m <sup>-3</sup>	3.1 ± 1.9	0.8 ± 0.5	2.0 ± 0.8	0.4 ± 0.3	3.3 ± 2.2	0.8 ± 0.5	3.6 ± 1.2	1.1 ± 0.4
Cd/ng m <sup>-3</sup>	1.4 ± 0.7	1.0 ± 0.5	0.8 ± 0.2	0.6 ± 0.2	1.6 ± 0.5	1.2 ± 0.4	1.8 ± 1.2	1.1 ± 0.7
V/ng m <sup>-3</sup>	1.1 ± 0.8	0.5 ± 0.4	0.6 ± 0.5	0.2 ± 0.2	1.2 ± 0.9	0.5 ± 0.4	1.3 ± 0.9	0.6 ± 0.4

Note: These data measured by ICP-MS.

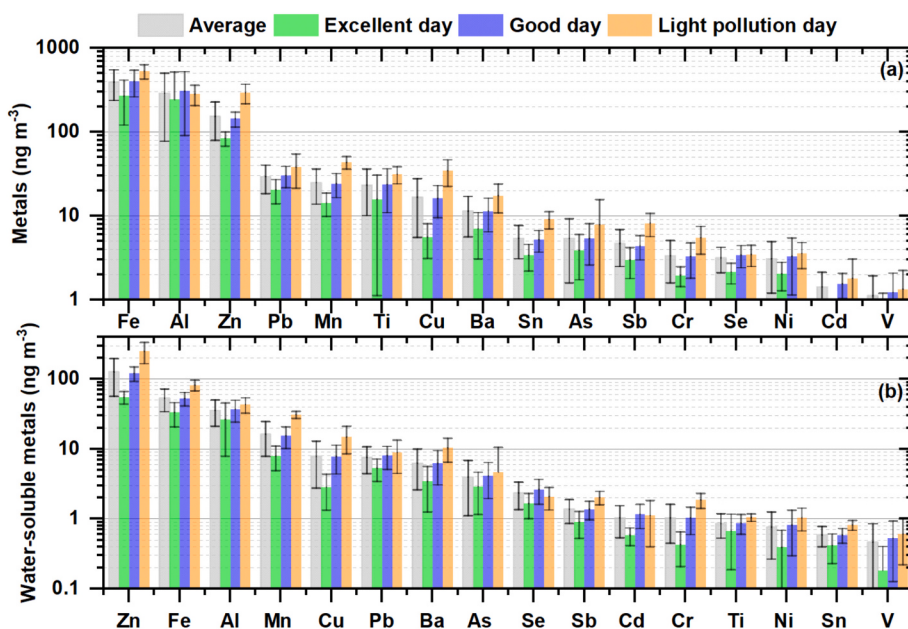


Fig. 1. Ranking of metal's total mass concentration and water-soluble portion.

The peak mass concentrations of Mn, Fe, and Cu were observed in coarse mode, but their size distributions exhibited slight differences. The peak mass concentrations of Mn and Fe were found in the sizes of 4.2–10.2 µm, while that of Cu was observed in the sizes of 2.1–4.2 µm. In contrast, water-soluble Mn, Fe, and Cu were predominantly distributed in fine mode, with peak concentrations occurring in the sizes of 0.73–1.4 µm. The observed differences in size distributions between metals and their water-soluble fractions were consistent with observations at other urban sites (Fang et al., 2017; Liu et al., 2022a; Lyu et al., 2018; Wang et al., 2015). These findings suggest distinct sources for these transition metals and their water-soluble fractions.

### 3.2. Metals solubilities from different sources

Metals in PM<sub>2.5</sub> with an average solubility below 20 % included Al, Ti, Fe, and Sn; between 20 and 40 % included V, Cr, Sb, Pb, and Ni; between 40 and 60 % included Ba and Cu, and higher than 60 % included Zn, As, Se, Cd, and Mn (Fig. 3a). Substantial variabilities in

metal solubilities have also been reported in previous studies conducted in urban areas of Europe and the United States. The low solubilities of crustal elements (Al, Ti, Fe) (<20 %) observed in the present study were consistent with previous findings; the solubilities of Cr and Pb (10–40 %) from our study were slightly higher than earlier reports. The solubilities of V, Ni, Cu, As, Cd, and Mn from our study fell within the wide range (20–80 %) reported in the literature (Badami et al., 2023; Heal et al., 2005; Manousakas et al., 2014). Solubilities were significantly higher for metals in the fine mode than in the coarse mode. Specifically, metals in the sizes of 0.41–0.73 µm and 0.73–1.4 µm exhibited higher solubilities than those in the ranges of <0.41 µm and 1.4–2.1 µm (Fig. 3b–e), which was consistent with observations in urban Beijing (Wang et al., 2015).

To understand the solubilities of the metals from different sources, PMF analysis was conducted using online XRF measurements of metal mass concentrations at 4 h intervals. Five major source factors were identified, including (1) non-exhaust emissions, (2) traffic emissions, (3) oil combustion, (4) coal combustion, and (5) soil dust. The chemical profiles for these source factors are presented in Fig. 4.

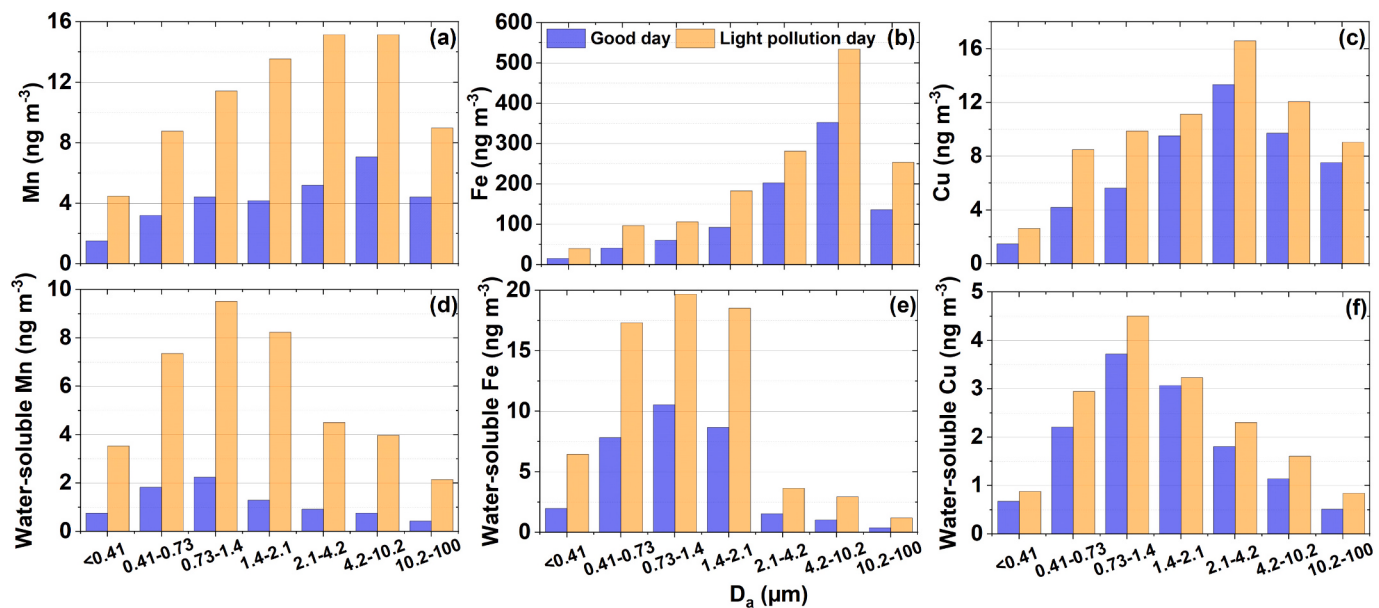


Fig. 2. Size distributions of transition metals (Mn, Fe, and Cu) mass concentrations on a typical lightly polluted day and a typical good day.

Factor 1 (non-exhaust emissions) was characterized by high Sn and Sb contents, comprising 61 % and 69 %, respectively, of their respective total mass concentrations (Fig. 4a). Previous studies in 2014 detected high levels of Sb, which was primarily attributed to coal combustion, with no detectable Sn at the SCIES site during the same season (Tao et al., 2017). However, a substantial decrease in PM<sub>2.5</sub>-bound Sb concentration was observed in 2019–2020, concurrent with the detection of Sn, suggesting a shift in Sb emission sources. Automotive brake pads typically contain approximately 6 % Sb<sub>2</sub>S<sub>3</sub> along with other metals such as Cu, Sn, Fe, and Zn, depending on the manufacturer (Martinez and Echeberria, 2016). The average Cu/Sb ratio from brake wear is generally <5.0. The Cu/Sb ratio in Guangzhou was 3.5 ± 1.7, strongly indicating that Sb originated from vehicle brake dust (Thorpe and Harrison, 2008). Notably, the Cu/Sb ratio in Factor 1 was <0.01, with high Fe concentrations, suggesting that Fe may have substituted for Cu in the braking system. Fe was the most abundant metal in Factor 1, consistent with its predominance in brake systems (Martinez and Echeberria, 2016). A moderate linear correlation ( $R^2 = 0.47$ ,  $p < 0.01$ ) between EC mass concentration and Factor 1 mass concentration (Fig. S5) further supports the link between these metals and traffic emissions. The widespread adoption of electric vehicles in Guangzhou in recent years likely explains the detection of Sn and the differentiation between Factor 1 and Factor 2 (traffic emissions). Therefore, to distinguish Factor 1 from conventional traffic emissions, we classified it as non-exhaust emissions.

Roadside observations have shown that the solubility of Sb in PM<sub>2.5</sub> and Sn in PM<sub>7.2</sub> was approximately 60 % and <3 %, respectively (Birmili et al., 2006; Oakes et al., 2016), likely due to the low solubility of Sn oxide in water and weak acids (Mori et al., 2002). Although the solubility of Sn (11 ± 2 %) was notably lower than that of Sb (30 ± 6 %) in this study, the solubility of Sb was evidently lower than the 60 % observed at the roadside site (Oakes et al., 2016). This difference may be attributed to the oxidation of Sb<sub>2</sub>S<sub>3</sub> to less soluble Sb<sub>2</sub>O<sub>3</sub> or Sb<sub>2</sub>O<sub>4</sub> at high temperatures (~400 °C) in brake pads, or even reduction reactions with Fe to form insoluble FeSb<sub>2</sub> or FeSb (Martinez and Echeberria, 2016).

Factor 2 (traffic emissions) exhibited high contents of Cr, Mn, Cu, Zn, and Ba, accounting for 54 %, 48 %, 61 %, 52 %, and 51 %, respectively, of their respective total mass concentrations (Fig. 4b). While these metals have been associated with metal smelting in Shanghai, they were primarily attributed to traffic emissions in the PRD region (Chang et al., 2018; Tao et al., 2023, 2017; Wang et al., 2022). This shift was likely due to the closure of all metal smelting plants in the PRD region over the past

20 years. Zn and Cu are in large quantities in engine oil and diesel, while Cr, Mn, and Ba are primarily in engine oil (Coufalik et al., 2019). Additionally, these metals are widely present in tires, brakes, road asphalt, and road paints (Thorpe and Harrison, 2008). A strong linear correlation ( $R^2 = 0.76$ ,  $p < 0.01$ ) between EC mass concentration and Factor 2 (traffic emissions) mass concentration in this study (Fig. S5) further supported the primary origin of these metals from traffic emissions. This finding was consistent with previous studies, indicating that EC in urban areas of the PRD region was predominantly derived from traffic emissions, mainly from gasoline vehicles (Tao et al., 2023, 2017). Despite undergoing high-temperature combustion, Zn and Cu exhibited significantly different solubilities (80 ± 11 % and 48 ± 9 %, respectively). The lower solubility of Cr (31 ± 8 %) might be attributed to its lower solubility in the sizes of 1.4–2.1 µm (Fig. 3d), potentially due to contributions from brake systems (Johansson et al., 2009). The solubility patterns of these metals correspond with roadside observations (Oakes et al., 2016), likely due to the limited interaction time between acidic constituents from urban traffic and atmospheric aerosols, which hinders further enhancement of their solubilities (Li et al., 2023).

Factor 3 (oil combustion) was identified by high V and Ni contents, comprising 79 % and 65 %, respectively, of their total mass concentrations (Fig. 4c). These metals, commonly used as indicators of ship sources, mainly stem from marine heavy oil fuel (Corbin et al., 2018; Viana et al., 2009; Yu et al., 2021; Zhao et al., 2021). The V/Ni ratio typically exceeds 2.5 in heavy fuel oil combustion emissions, and below 2.5 in gasoline vehicles emissions (Corbin et al., 2018; Ray and Das, 2023). The average V/Ni ratio was 0.35 ± 0.15 in Guangzhou in 2019–2020, significantly lower than the average V/Ni ratio of 2.0 observed at the SCIES site during the same season in 2014 (Tao et al., 2017). The average V/Ni ratio in Factor 3 was 0.72, substantially lower than 2.5, as seen in the 2014 source profile of ship emissions (Tao et al., 2017). These findings confirmed the identification of Factor 3 as oil combustion. The results also suggested that shore power measures in recent years at ports in the PRD region may have significantly reduced emissions from berthed vessels, thereby increasing the relative contribution of traffic emissions to Ni and V mass concentrations. The solubilities of Ni and V in this study were 37 ± 12 % and 24 ± 7 %, respectively, which are consistent with the mean solubilities of Ni and V from direct oil combustion emissions, which were reported as approximately 53 % and 20 %, respectively (Galbreath et al., 2000; Shafer et al., 2012).

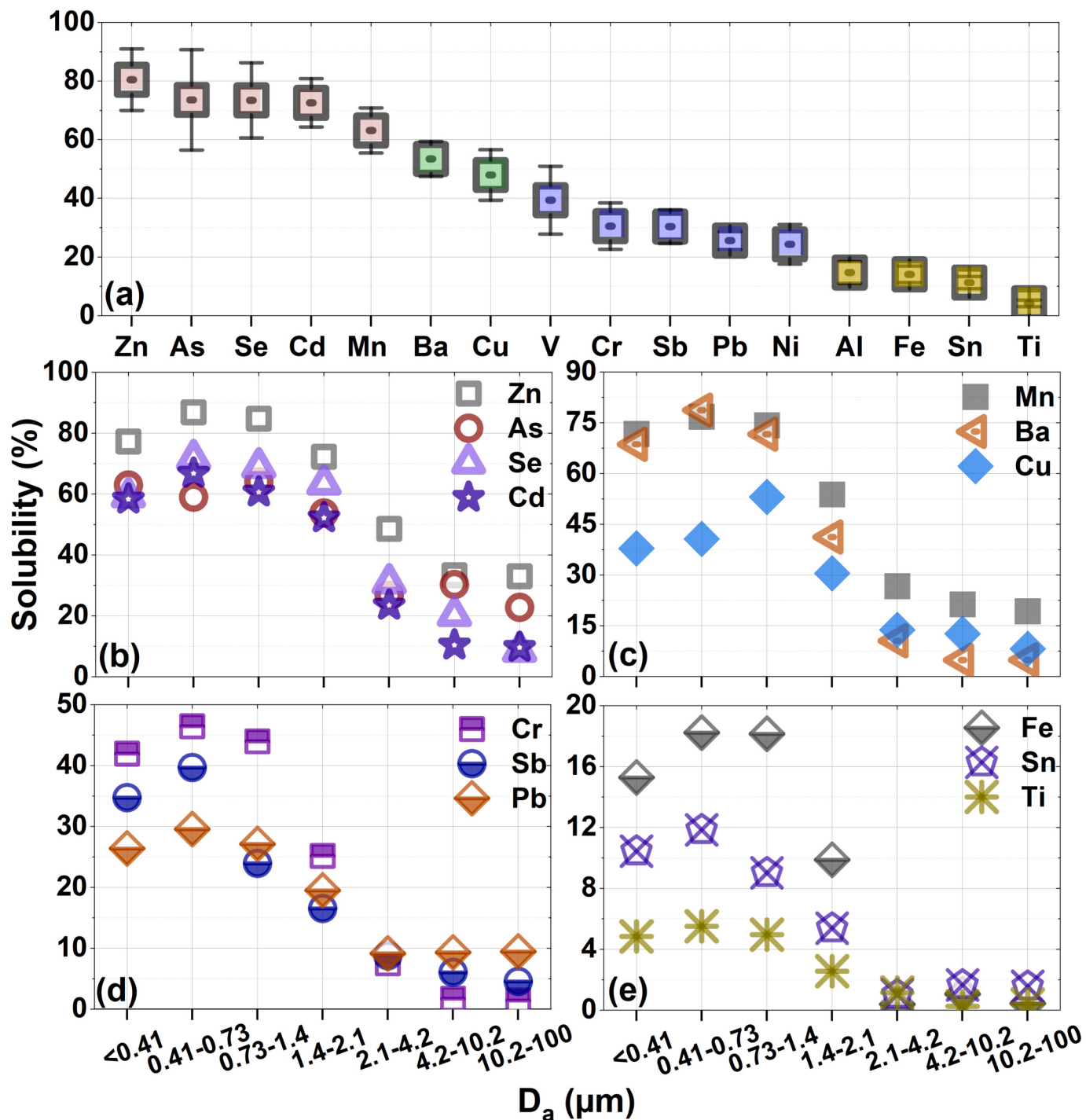


**Fig. 3.** (a) Ranking of metal solubility in  $\text{PM}_{2.5}$ , and (b, c, d, and e) size distributions of metal solubility.

Factor 4 (coal combustion) was characterized by high As, Se, Cd, and Pb contents, constituting 72 %, 66 %, 62 %, and 61 %, respectively, of their respective total mass concentrations (Fig. 4d). These metals predominantly originate from coal combustion, though Sb was not found in coal combustion in this study (Liu et al., 2018; Tian et al., 2013; Xu et al., 2004). Previous studies on metal leaching in coal fly ash had shown that As, Se, and Cd generally exhibit low solubilities, with <20 % solubility for As and Se even under weakly acidic conditions (Jegadeesan et al., 2008; Narukawa et al., 2005; Shivpuri et al., 2012). However, in our study, As, Se, and Cd exhibited significantly higher solubilities (>73 %), far exceeding those reported for coal fly ash. These elevated solubilities in the atmospheric environment can be attributed to acidification during

transport, given the concurrent emissions of large quantities of acidic substances from coal combustion (Song et al., 2024). Additionally, the low solubility of Pb (26 %) is due to its strong association with silicates in coal combustion (Kim and Kazonich, 2004).

Factor 5 (soil dust) was characterized by high Ti and Fe contents, accounting for 73 % and 52 %, respectively, of their respective total mass concentrations (Fig. 4e). Although Al, Si, and Ca were not used as inputs for the PMF analysis, these species correlated well with Ti (Fig. S6), suggesting that this factor likely contains high contents of Al, Si, Ca, Ti, and Fe, all of which are typical crustal metals in the source profile of soil dust (Sun et al., 2019; Zhang et al., 2014). While Fe from soil dust generally exhibits low solubility (<3 %) and Fe from

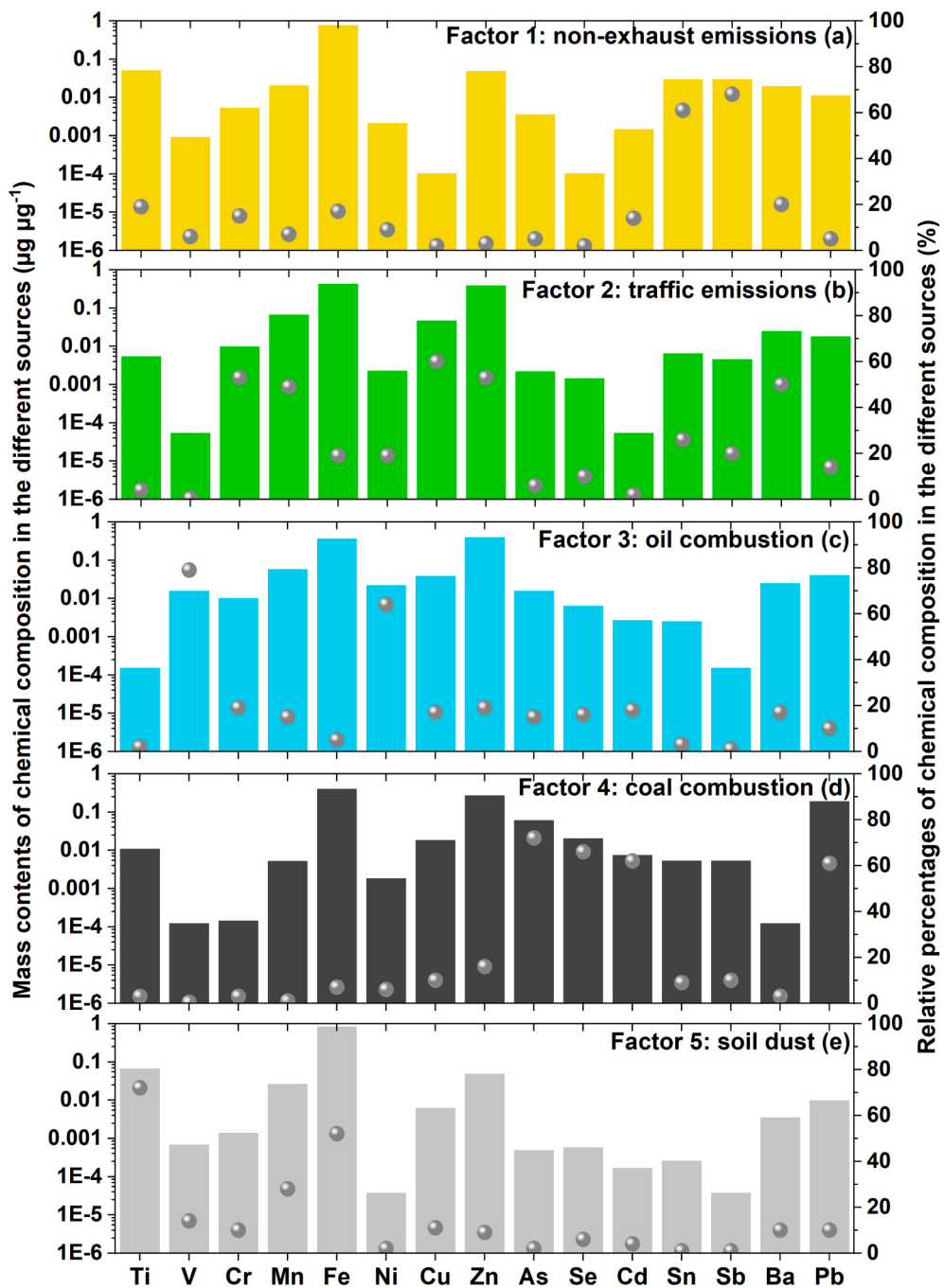


**Fig. 4.** Five source factors of metals (bars) resolved from the PMF model, with percentage contributions (grey dots) from each source factor.

combustion sources remains relatively insoluble (<6 %), the observed solubilities of Fe and Al in this study were approximately 13 %, likely due to atmospheric heterogeneous chemical processes (Liu et al., 2022a; Zhang et al., 2022; Zhu et al., 2022). Additionally, Ti exhibited a solubility of only 4 %, due to the high stability of  $\text{TiO}_2$  even under acidic conditions (Tyler and Olsson, 2001).

Overall, the solubilities of heavy metals from coal combustion and crustal metals from natural sources were relatively low at the emission point, but increased significantly after undergoing atmospheric physical and chemical processes. While heavy metals from coal combustion can achieve solubilities exceeding 70 % (except for Pb at 26 %), crustal metals from natural sources typically limit their solubilities to 5–15 %. Metals from non-exhaust emissions, traffic emissions, and oil combustion exhibited solubilities comparable to those from directly emitted

sources, possibly due to the close association of these sources with vehicles, resulting in relatively short atmospheric processing times and limited increases in solubility. These findings underscore significant disparities in solubility between metals from anthropogenic and natural sources and highlight the substantial enhancement in solubility of metals subject to atmospheric physical and chemical processes.

### 3.3. Influence of atmospheric physicochemical processes on metal solubilities

As discussed in Section 3.2, metal solubility is primarily governed by source categories (anthropogenic or natural) and inherent physicochemical properties (Birmili et al., 2006; Izquierdo and Querol, 2012; Liu et al., 2022a; Oakes et al., 2016; Stumm and Morgan, 2012; Zhu

et al., 2022). Additionally, atmospheric physicochemical processes significantly influence metal solubility (Desboeufs et al., 2005; Liu et al., 2022a; Oakes et al., 2016; Zhu et al., 2022). Experiments on metal leaching from coal fly ash and atmospheric particulate matter have consistently shown that the application of organic acids can substantially enhance metal solubility, particularly when accompanied by a decrease in the pH of the leaching solution (Chen et al., 2012; Chen and Grassian, 2013; Li et al., 2022; Shivpuri et al., 2012). These findings further support the idea that atmospheric physicochemical processes, including acidification, organic acid complexation, and heterogeneous reactions, can markedly alter metal solubility (Chen and Grassian, 2013; Srinivas et al., 2014; Winton et al., 2016; Wozniak et al., 2013; Zhang et al., 2022). Consequently, this study employed correlation analysis to investigate the dependency of metal solubility on aerosol acidity (pH, including  $H^+$  and ALWC), oxalate, and WSOC.

As shown in Fig. 5, there were negative correlations between the solubilities of Cu, As, Se, Cd, Sn, Sb, and Pb and aerosol pH ( $R < -0.52$ ,  $p < 0.01$ ), as well as ALWC ( $R < -0.39$ ,  $p < 0.05$ , except for Cu), while positive correlations were observed with  $H^+$  mass concentration ( $R > 0.59$ ,  $p < 0.01$ ). These results indicate that increased aerosol acidity enhances the solubilities of these metals. Conversely, positive correlations were found between the solubilities of V, Cr, Mn, Ni, Zn, and Ba and oxalate ( $R > 0.53$ ,  $p < 0.01$ ) as well as WSOC ( $R > 0.45$ ,  $p < 0.01$ ), suggesting that complexation with organic acids enhances their solubilities. Interestingly, the solubility of these metals, though linked to aerosol acidity, appears unrelated to oxalic acid or WSOC, likely because oxalic acid preferentially forms the oxalate ion ( $C_2O_4^{2-}$ ) at higher pH, which can chelate metal cations (Verma et al., 2019).

According to the regression slopes for Cu, As, Se, Cd, Sn, Sb, and Pb against aerosol pH and  $H^+$  mass concentrations, their solubilities would increase on average by 15 %, 30 %, 28 %, 10 %, 3 %, 10 %, and 3 %, respectively. For V, Cr, Mn, Ni, Zn, and Ba, the solubilities increased on average by 25 %, 15 %, 18 %, 13 %, 25 %, and 15 %, respectively, when regressed against oxalate and WSOC. These results suggest that organic acids primarily influence the solubility of transition metals, while non-transition metals are mainly affected by aerosol acidity. In summary, increases in aerosol acidity, oxalate, and WSOC would result in solubility increases of <10 % for Cd, Sn, Sb, and Pb; 10–20 % for Cu, Cr, Mn, Ni, and Ba; and 20–30 % for As, Se, and Zn. These findings underscore the significant impact of atmospheric physicochemical processes on metal solubility and highlight the varying degrees of influence on different metals.

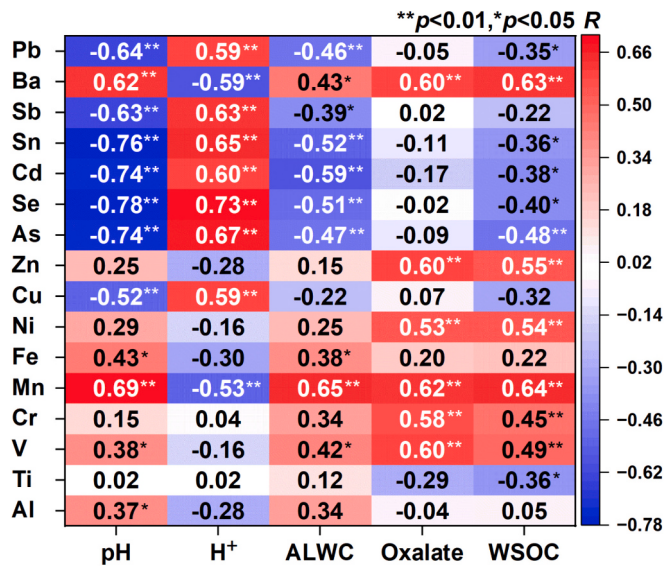


Fig. 5. Correlation coefficients ( $R$ ) between metal solubility and pH value,  $H^+$ , oxalate, and WSOC mass concentrations.

Intriguingly, the solubilities of Al and Fe exhibited weak positive correlations with aerosol pH ( $R = 0.37$ ,  $p < 0.05$  for Al and  $R = 0.43$ ,  $p < 0.05$  for Fe) and no correlation with oxalate or WSOC concentrations. In addition, the solubility of Fe exhibited a weak positive correlation with ALWC ( $R = 0.38$ ,  $p < 0.05$ ), suggesting the solubility of Fe might be related to heterogeneous reactions (Liu et al., 2022a). Similarly, Ti exhibited no correlation with aerosol pH, but only a weak positive correlation with WSOC mass concentration ( $R = -0.36$ ,  $p < 0.05$ ). These findings indicate that other factors besides acidification and organic acid complexation may also influence the solubilities of Al, Ti, and Fe.

It is worth noting that during the observation period, a severe dust storm occurred from October 26 to 29, 2019, in northern China, leading to elevated PM<sub>10</sub> and PM<sub>2.5</sub> concentrations in northern Chinese cities (Fig. S7) (Wang et al., 2020). Consequently, a substantial increase in the mass concentrations of crustal metals (Si, Al, Fe, and Ti) in PM<sub>2.5</sub> was observed in the PRD region due to the long-range transport of dust storm-produced particles (Fig. 6a, b, and c). Notably, Si mass concentration exhibited a more significant increase than those of Al, Fe, and Ti, mainly due to higher Si content in dust particles (Zhang et al., 2014). During the dust event, the mass concentrations of Al, Fe, and Ti increased substantially (by 209 %, 44 %, and 101 %, respectively), while the mass concentrations of their respective water-soluble fractions changed much less (67 %, -11 %, and 42 %, respectively). Consequently, the solubilities of Al, Fe, and Ti were significantly lower during the dust storm period compared to the whole observation period (Fig. 6d). These results indicate substantial impacts of dust storms originating in Northern China on the solubilities of crustal metals in South China (Liu et al., 2022a).

The correlation analysis results presented above were re-examined after excluding the influence of dust storm particles. Upon exclusion of days affected by the dust event, the positive correlations between the solubilities of Al and Ti and aerosol acidity (aerosol pH or  $H^+$  concentration) indeed strengthened ( $p < 0.05$ ), while significantly negative correlations with WSOC (or oxalate) were observed ( $p < 0.05$ ) (Fig. 7). These findings suggest that the solubilities of Al and Ti during non-dust periods are closely linked to aerosol acidity rather than complexation with organic acids.

Robust correlations were also observed between Fe solubility and both aerosol acidity ( $R = -0.41$ ,  $p < 0.05$  for aerosol pH;  $R = 0.51$ ,  $p < 0.05$  for  $H^+$ ) and oxalate concentration ( $R = 0.47$ ,  $p < 0.05$ ) after excluding the influence of dust storms (Fig. 7). This indicates that Fe

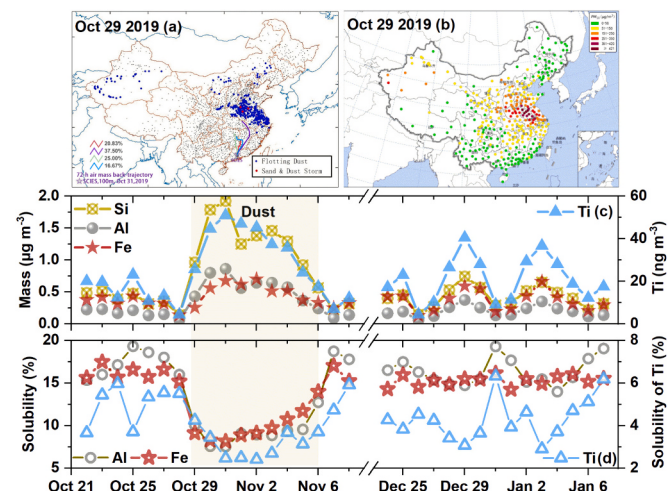
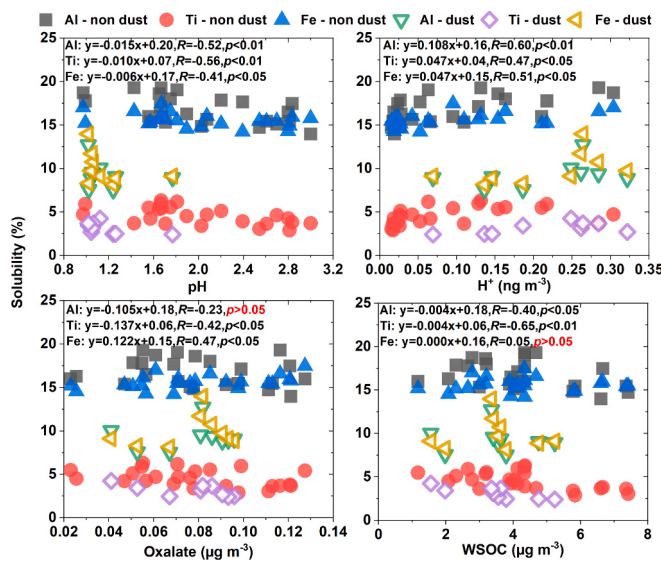


Fig. 6. (a) Spatial distributions of floating dust and dust storms on October 29, 2019, along with the 72-hour air mass back-trajectory at 100 m height on October 31, 2019; (b) Spatial distributions of PM<sub>10</sub> mass concentrations on October 29, 2019; (c) Daily variations in crustal metal mass concentrations; and (d) Daily variations in the solubility of typical crustal metals (Al, Ti, and Fe).



**Fig. 7.** Correlations between the solubility of crustal elements (Al, Ti, and Fe) and pH value,  $H^+$ , oxalate, and WSOC after excluding the dust storm.

solubility is indeed influenced by both aerosol acidity and oxalate concentration (Tao and Murphy, 2019; Yang and Weber, 2022; Zhang et al., 2023). The slight difference in correlation coefficients between Fe solubility and oxalate concentration and between Fe solubility and aerosol acidity suggests that both factors play equally important roles in determining Fe solubility.

As illustrated in Fig. 8, when the aerosol pH drops below 2.0, the

enhanced solubility of Fe is primarily driven by increased  $H^+$  concentration and decreased ALWC concentration, indicating that aerosol acidity is the dominant factor controlling Fe solubility. Conversely, when the aerosol pH exceeds 2.0, the increased solubility of Fe is mainly attributed to higher concentrations of oxalate or WSOC and ALWC, suggesting that complexation with organic acids becomes the primary control. This is because higher aerosol pH and ALWC concentration favor the ionic form of organic acids, facilitating complexation with metal ions (Verma et al., 2019). Notably, even when the aerosol pH is below 2.0, if the  $H^+$  concentration is high but the ALWC concentration is low, Fe solubility remains relatively low, highlighting the importance of heterogeneous acidification of metals (Liu et al., 2022a; Zhang et al., 2022; Zhu et al., 2022). Moreover, Fe solubility can still increase significantly when both  $H^+$  and ALWC concentrations are low at a pH below 2.0, but the oxalate concentration is high.

#### 4. Conclusions

This study investigated the solubilities of 16 metals (Al, Ti, V, Cr, Mn, Fe, Ni, Cu, Zn, As, Se, Cd, Sn, Sb, Ba, and Pb) in  $PM_{2.5}$  as well as potential factors influencing their solubilities in urban Guangzhou, South China during the dry season of 2019–2020. Five distinct sources contributing to these metals were identified, including non-exhaust emissions, traffic emissions, oil combustion, coal combustion, and soil dust. Source apportionment results for these metals align with previous studies, except for Sb and Sn, which primarily came from the non-exhaust emissions rather than coal combustion in this study. Notably, crustal metals (e.g., Al, Ti, and Fe) exhibit significantly lower solubility than those that originated from fossil fuel combustion (e.g., As, Se, Cd, and Pb). The solubilities of these metals are largely determined by the

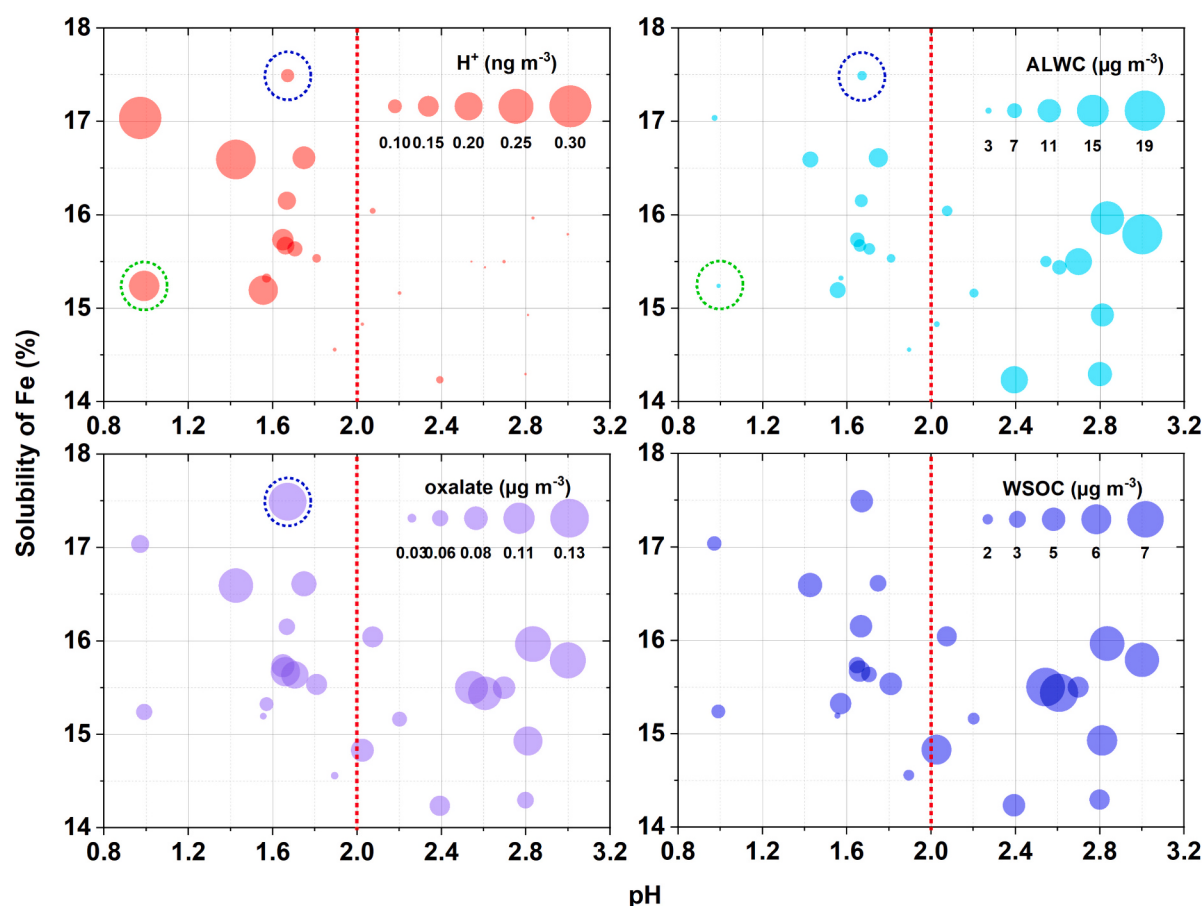


**Fig. 8.** Correlation between Fe solubility and pH value under different  $H^+$ , ALWC, oxalate, and WSOC mass concentrations.

inherent properties of their sources, but are also influenced by atmospheric physicochemical processes. The increased solubilities of Cu, As, Se, Cd, Sn, Sb, and Pb may be linked to heightened aerosol acidity, while the enhanced solubilities of V, Cr, Mn, Ni, Zn, and Ba are associated with organic acid complexation. Notably, the solubilities of Al and Ti are likely predominantly influenced by aerosol acidity, whereas Fe solubility is affected by aerosol acidity at lower pH levels and organic acid complexation at higher pH levels. Reducing emissions of volatile organic compounds, which are precursors of organic acids, would decrease organic acid content in PM<sub>2.5</sub> and lower the solubilities of transition metals, which may reduce the health risks associated with PM<sub>2.5</sub>.

#### CRediT authorship contribution statement

**Zhisheng Zhang:** Writing – original draft, Investigation, Formal analysis, Data curation. **Jun Tao:** Writing – review & editing, Supervision, Investigation, Funding acquisition, Data curation, Conceptualization. **Leiming Zhang:** Writing – review & editing, Investigation. **Bangkai Hu:** Software, Data curation. **Ming Liu:** Methodology, Formal analysis. **Fuli Nie:** Methodology, Formal analysis, Data curation. **Haitao Lu:** Methodology, Formal analysis, Data curation. **Laiguo Chen:** Writing – review & editing, Resources. **Yunfei Wu:** Writing – review & editing, Investigation. **Duohong Chen:** Writing – review & editing, Resources. **Boguang Wang:** Writing – review & editing. **Huizheng Che:** Writing – review & editing, Resources, Data curation.

#### Declaration of competing interest

The authors declare the following financial interests/personal relationships which may be considered as potential competing interests: Jun TAO reports financial support was provided by Jinan University Institute for Environment and Climate Research. If there are other authors, they declare that they have no known competing financial interests or personal relationships that could have appeared to influence the work reported in this paper.

#### Data availability

Data used in this study are available from Jun Tao ([taojun@jnu.edu.cn](mailto:taojun@jnu.edu.cn)).

#### Acknowledgments

This study was supported by the National Natural Science Foundation of China (No. 41875160).

#### Appendix A. Supplementary data

Supplementary data to this article can be found online at <https://doi.org/10.1016/j.scitotenv.2024.175807>.

#### References

- Badami, M.M., Tohidi, R., Jalali Farahani, V., Sioutas, C., 2023. Size-segregated source identification of water-soluble and water-insoluble metals and trace elements of coarse and fine PM in central Los Angeles. *Atmos. Environ.* 310, 119984 <https://doi.org/10.1016/j.atmosenv.2023.119984>.
- Birmili, W., Allen, A.G., Bary, F., Harrison, R.M., 2006. Trace metal concentrations and water solubility in size-fractionated atmospheric particles and influence of road traffic. *Environ. Sci. Technol.* 40, 1144–1153. <https://doi.org/10.1021/es0486925>.
- Chang, Y., Huang, K., Xie, M., Deng, C., Zou, Z., Liu, S., Zhang, Y., 2018. First long-term and near real-time measurement of trace elements in China's urban atmosphere: temporal variability, source apportionment and precipitation effect. *Atmos. Chem. Phys.* 18, 11793–11812. <https://doi.org/10.5194/acp-18-11793-2018>.
- Charrier, J.G., Anastasio, C., 2012. On dithiothreitol (DTT) as a measure of oxidative potential for ambient particles: evidence for the importance of soluble transition metals. *Atmos. Chem. Phys.* 12, 9321–9333. <https://doi.org/10.5194/acp-12-9321-2012>.
- Chen, H., Grassian, V.H., 2013. Iron dissolution of dust source materials during simulated acidic processing: the effect of sulfuric, acetic, and oxalic acids. *Environ. Sci. Technol.* 47, 10312–10321. <https://doi.org/10.1021/es401285s>.
- Chen, H., Laskin, A., Baltrušaitis, J., Gorski, C.A., Scherer, M.M., Grassian, V.H., 2012. Coal fly ash as a source of iron in atmospheric dust. *Environ. Sci. Technol.* 46, 2112–2120. <https://doi.org/10.1021/es204102f>.
- Cheng, I., Al Mamun, A., Zhang, L., 2021. A synthesis review on atmospheric wet deposition of particulate elements: scavenging ratios, solubility, and flux measurements. *Environ. Rev.* 29, 340–353. <https://doi.org/10.1139/er-2020-0118>.
- Corbin, J.C., Mensah, A.A., Pieber, S.M., Orasche, J., Michalke, B., Zanatta, M., Czech, H., Massabò, D., Buatier de Mongeot, F., Mennucci, C., El Haddad, I., Kumar, N.K., Stengel, B., Huang, Y., Zimmermann, R., Prévôt, A.S.H., Gysel, M., 2018. Trace metals in soot and PM2.5 from heavy-fuel-oil combustion in a marine engine. *Environ. Sci. Technol.* 52, 6714–6722. <https://doi.org/10.1021/acs.est.8b01764>.
- Coufalík, P., Matoušek, T., Krůmal, K., Vojtíšek-Lom, M., Beránek, V., Mikuška, P., 2019. Content of metals in emissions from gasoline, diesel, and alternative mixed biofuels. *Environ. Sci. Pollut. Res.* 26, 29012–29019. <https://doi.org/10.1007/s11356-019-06144-4>.
- Desboeufs, K.V., Sofikitis, A., Losno, R., Colin, J.L., Asset, P., 2005. Dissolution and solubility of trace metals from natural and anthropogenic aerosol particulate matter. *Chemosphere* 58, 195–203. <https://doi.org/10.1016/j.chemosphere.2004.02.025>.
- Fang, T., Guo, H., Verma, V., Peltier, R.E., Weber, R.J., 2015. PM2.5 water-soluble elements in the southeastern United States: automated analytical method development, spatiotemporal distributions, source apportionment, and implications for health studies. *Atmos. Chem. Phys.* 15, 11667–11682. <https://doi.org/10.5194/acp-15-11667-2015>.
- Fang, T., Verma, V., Bates, J.T., Abrams, J., Klein, M., Strickland, M.J., Sarnat, S.E., Chang, H.H., Mulholland, J.A., Tolbert, P.E., Russell, A.G., Weber, R.J., 2016. Oxidative potential of ambient water-soluble PM2.5 in the southeastern United States: contrasts in sources and health associations between ascorbic acid (AA) and dithiothreitol (DTT) assays. *Atmos. Chem. Phys.* 16, 3865–3879. <https://doi.org/10.5194/acp-16-3865-2016>.
- Fang, T., Guo, H., Zeng, L., Verma, V., Nenes, A., Weber, R.J., 2017. Highly acidic ambient particles, soluble metals, and oxidative potential: a link between sulfate and aerosol toxicity [WWW document]. ACS Publications. <https://doi.org/10.1021/acs.est.6b0151>.
- Fu, H., Cwiertny, D.M., Carmichael, G.R., Scherer, M.M., Grassian, V.H., 2010. Photoreductive dissolution of Fe-containing mineral dust particles in acidic media. *J. Geophys. Res. Atmos.* 115 <https://doi.org/10.1029/2009JD012702>.
- Fu, X., Guo, H., Wang, X., Ding, X., He, Q., Liu, T., Zhang, Z., 2015. PM2.5 acidity at a background site in the Pearl River Delta region in fall-winter of 2007–2012. *J. Hazard. Mater.* 286, 484–492. <https://doi.org/10.1016/j.jhazmat.2015.01.022>.
- Fu, S., Yue, D., Lin, W., Hu, Q., Yuan, L., Zhao, Y., Zhai, Y., Mai, D., Zhang, H., Wei, Q., He, L., 2021. Insights into the source-specific health risk of ambient particle-bound metals in the Pearl River Delta region, China. *Ecotoxicology and Environmental Safety* 224, 112642. <https://doi.org/10.1016/j.ecoenv.2021.112642>.
- Galbreath, Kevin C., Toman, D.L., Zygarlicke, C.J., Huggins, F.E., Huffman, G.P., Wong, J.L., 2000. Nickel speciation of residual oil fly ash and ambient particulate matter using X-ray absorption spectroscopy. *J. Air Waste Manage. Assoc.* 50, 1876–1886. <https://doi.org/10.1080/10473289.2000.10464230>.
- Galon-Negrú, A.G., Olariu, R.I., Arsene, C., 2019. Size-resolved measurements of PM2.5 water-soluble elements in Iasi, north-eastern Romania: seasonality, source apportionment and potential implications for human health. *Sci. Total Environ.* 695, 133839 <https://doi.org/10.1016/j.scitotenv.2019.133839>.
- Hans Wedepohl, K., 1995. The composition of the continental crust. *Geochim. Cosmochim. Acta* 59, 1217–1232. [https://doi.org/10.1016/0016-7037\(95\)00038-2](https://doi.org/10.1016/0016-7037(95)00038-2).
- He, L., Wang, S., Liu, M., Chen, Z., Xu, J., Dong, Y., 2023. Transport and transformation of atmospheric metals in ecosystems: a review. *Journal of Hazardous Materials Advances* 9, 100218. <https://doi.org/10.1016/j.hazadv.2022.100218>.
- Heal, M.R., Hibbs, L.R., Agius, R.M., Beverland, I.J., 2005. Total and water-soluble trace metal content of urban background PM10, PM2.5 and black smoke in Edinburgh, UK. *Atmospheric Environment* 39, 1417–1430. <https://doi.org/10.1016/j.atmosenv.2004.11.026>.
- Huang, W., Zhang, Z., Huang, J., Tao, J., Zhou, Z., Yuan, Z., Yang, Y., Wang, B., 2023. High contribution of non-exhaust emission to health risk of PM2.5-bound toxic metals in an urban atmosphere in south China. *Atmos. Environ.* 306, 119824 <https://doi.org/10.1016/j.atmosenv.2023.119824>.
- Ito, T., Nenes, A., Johnson, M.S., Meskhidze, N., Deutsch, C., 2016. Acceleration of oxygen decline in the tropical Pacific over the past decades by aerosol pollutants. *Nat. Geosci.* 9, 443–447. <https://doi.org/10.1038/ngeo2717>.
- Izquierdo, M., Querol, X., 2012. Leaching behaviour of elements from coal combustion fly ash: an overview. *Int. J. Coal Geol.* 94, 54–66. <https://doi.org/10.1016/j.coal.2011.10.006>.
- Jegadeesan, G., Al-Abed, S.R., Pinto, P., 2008. Influence of trace metal distribution on its leachability from coal fly ash. *Fuel* 87, 1887–1893. <https://doi.org/10.1016/j.fuel.2007.12.007>.
- Jia, S., Chen, W., Zhang, Q., Krishnan, P., Mao, J., Zhong, B., Huang, M., Fan, Q., Zhang, J., Chang, M., Yang, L., Wang, X., 2020. A quantitative analysis of the driving factors affecting seasonal variation of aerosol pH in Guangzhou, China. *Science of The Total Environment* 725, 138228. <https://doi.org/10.1016/j.scitotenv.2020.138228>.
- Johansson, C., Norman, M., Burman, L., 2009. Road traffic emission factors for heavy metals. *Atmospheric Environment*, *Urban Air Quality* 43, 4681–4688. <https://doi.org/10.1016/j.atmosenv.2008.10.024>.

- Kim, A.G., Kazonich, G., 2004. The silicate/non-silicate distribution of metals in fly ash and its effect on solubility. *Fuel* 83, 2285–2292. <https://doi.org/10.1016/j.fuel.2004.06.005>.
- Li, T., Wang, Y., Li, W.J., Chen, J.M., Wang, T., Wang, W.X., 2015. Concentrations and solubility of trace elements in fine particles at a mountain site, southern China: regional sources and cloud processing. *Atmos. Chem. Phys.* 15, 8987–9002. <https://doi.org/10.5194/acp-15-8987-2015>.
- Li, W., Xu, L., Liu, X., Zhang, J., Lin, Y., Yao, X., Gao, H., Zhang, D., Chen, J., Wang, W., Harrison, R.M., Zhang, X., Shao, L., Fu, P., Nenes, A., Shi, Z., 2017. Air pollution–aerosol interactions produce more bioavailable iron for ocean ecosystems. *Sci. Adv.* 3, e1601749 <https://doi.org/10.1126/sciadv.1601749>.
- Li, R., Zhang, H., Wang, F., He, Y., Huang, C., Luo, L., Dong, S., Jia, X., Tang, M., 2022. Mass fractions, solubility, speciation and isotopic compositions of iron in coal and municipal waste fly ash. *Sci. Total Environ.* 838, 155974 <https://doi.org/10.1016/j.scitotenv.2022.155974>.
- Li, R., Dong, S., Huang, C., Yu, F., Wang, F., Li, X., Zhang, H., Ren, Y., Guo, M., Chen, Q., Ge, B., Tang, M., 2023. Evaluating the effects of contact time and leaching solution on measured solubilities of aerosol trace metals. *Appl. Geochem.* 148, 105551 <https://doi.org/10.1016/j.apgeochem.2022.105551>.
- Liu, Y., Xing, J., Wang, S., Fu, X., Zheng, H., 2018. Source-specific speciation profiles of PM<sub>2.5</sub> for heavy metals and their anthropogenic emissions in China. *Environ. Pollut.* 239, 544–553. <https://doi.org/10.1016/j.envpol.2018.04.047>.
- Liu, L., Li, W., Lin, Q., Wang, Y., Zhang, J., Zhu, Y., Yuan, Q., Zhou, S., Zhang, D., Baldo, C., Shi, Z., 2022a. Size-dependent aerosol iron solubility in an urban atmosphere. *npj Clim Atmos Sci* 5, 53. <https://doi.org/10.1038/s41612-022-00277-z>.
- Liu, M., Wang, W., Li, J., Wang, T., Xu, Z., Song, Y., Zhang, W., Zhou, L., Lian, C., Yang, J., Li, Y., Sun, Y., Tong, S., Guo, Y., Ge, M., 2022b. High fraction of soluble trace metals in fine particles under heavy haze in central China. *Sci. Total Environ.* 841, 156771 <https://doi.org/10.1016/j.scitotenv.2022.156771>.
- Lyu, Y., Guo, H., Cheng, T., Li, X., 2018. Particle size distributions of oxidative potential of lung-deposited particles: assessing contributions from quinones and water-soluble metals. *Environ. Sci. Technol.* 52, 6592–6600. <https://doi.org/10.1021/acs.est.7b06686>.
- Mahowald, N.M., Hamilton, D.S., Mackey, K.R.M., Moore, J.K., Baker, A.R., Scanza, R.A., Zhang, Y., 2018. Aerosol trace metal leaching and impacts on marine microorganisms. *Nat. Commun.* 9, 2614. <https://doi.org/10.1038/s41467-018-04970-7>.
- Mamun, A.A., Cheng, I., Zhang, L., Dabek-Zlotorzynska, E., Charland, J.-P., 2019. Overview of size distribution, concentration, and dry deposition of airborne particulate elements measured worldwide. *Environ. Rev.* 1–12. <https://doi.org/10.1139/er-2019-0035>.
- Manousakas, M., Papaefthymiou, H., Eleftheriadis, K., Katsanou, K., 2014. Determination of water-soluble and insoluble elements in PM<sub>2.5</sub> by ICP-MS. *Sci. Total Environ.* 493, 694–700. <https://doi.org/10.1016/j.scitotenv.2014.06.043>.
- Martinez, A.M., Echeberria, J., 2016. Towards a better understanding of the reaction between metal powders and the solid lubricant Sb<sub>2</sub>S<sub>3</sub> in a low-metallic brake pad at high temperature. *Wear* 348–349, 27–42. <https://doi.org/10.1016/j.wear.2015.11.014>.
- Mori, M., Miura, K., Sasaki, T., Ohtsuka, T., 2002. Corrosion of tin alloys in sulfuric and nitric acids. *Corros. Sci.* 44, 887–898. [https://doi.org/10.1016/S0010-938X\(01\)00094-4](https://doi.org/10.1016/S0010-938X(01)00094-4).
- Narukawa, T., Takatsu, A., Chiba, K., Riley, K.W., French, D.H., 2005. Investigation on chemical species of arsenic, selenium and antimony in fly ash from coal fuel thermal power stations. *J. Environ. Monit.* 7, 1342–1348. <https://doi.org/10.1039/B509817C>.
- Nordberg, G.F., Costa, M., 2021. *Handbook on the Toxicology of Metals: Volume I: General Considerations*.
- Oakes, M.M., Burke, J.M., Norris, G.A., Kovalcik, K.D., Pancras, J.P., Landis, M.S., 2016. Near-road enhancement and solubility of fine and coarse particulate matter trace elements near a major interstate in Detroit, Michigan. *Atmos. Environ.* 145, 213–224. <https://doi.org/10.1016/j.atmosenv.2016.09.034>.
- Qureshi, S., Dutkiewicz, V.A., Khan, A.R., Swami, K., Yang, K.X., Husain, L., Schwab, J.J., Demerjian, K.L., 2006. Elemental composition of PM<sub>2.5</sub> aerosols in Queens, New York: solubility and temporal trends. *Atmos. Environ.* 40, 238–251. <https://doi.org/10.1016/j.atmosenv.2005.12.070>.
- Ray, I., Das, R., 2023. A lingering legacy of leaded gasoline in Southeast Asia. *Communications Earth & Environment* 4, 468. <https://doi.org/10.1038/s43247-023-01135-3>.
- Reeder, R.J., Schoonen, M.A.A., Lanzirotti, A., 2006. Metal speciation and its role in bioavailability and bioavailability. *Rev. Mineral. Geochem.* 64, 59–113. <https://doi.org/10.2138/rmg.2006.64.3>.
- Shafer, M.M., Toner, B.M., Overdier, J.T., Schauer, J.J., Fakra, S.C., Hu, S., Herner, J.D., Ayala, A., 2012. Chemical speciation of vanadium in particulate matter emitted from diesel vehicles and urban atmospheric aerosols. *Environ. Sci. Technol.* 46, 189–195. <https://doi.org/10.1021/es200463c>.
- Shi, Z., Krom, M.D., Bonneville, S., Benning, L.G., 2015. Atmospheric processing outside clouds increases soluble iron in mineral dust. *Environ. Sci. Technol.* 49, 1472–1477. <https://doi.org/10.1021/es504623x>.
- Shi, J., Guan, Y., Ito, A., Gao, H., Yao, X., Baker, A.R., Zhang, D., 2020. High production of soluble iron promoted by aerosol acidification in fog. *Geophys. Res. Lett.* 47 <https://doi.org/10.1029/2019GL086124>.
- Shivpuri, K.K., B., L., Kulkarni, D.A., Dikshit, A.K., 2012. Metal leaching potential in coal fly ash. *AJEE* 1, 21–27. <https://doi.org/10.5923/j.ajee.20110101.04>.
- Song, X., Wu, D., Chen, X., Ma, Z., Li, Q., Chen, J., 2024. Toxic potencies of particulate matter from typical industrial plants mediated with acidity via metal dissolution. *Environ. Sci. Technol.* 58, 6736–6743. <https://doi.org/10.1021/acs.est.4c00929>.
- Sørensen, M., Schins, R.P.F., Hertel, O., Loft, S., 2005. Transition metals in personal samples of PM<sub>2.5</sub> and oxidative stress in human volunteers. *Cancer Epidemiol. Biomarkers Prev.* 14, 1340–1343. <https://doi.org/10.1158/1055-9965.EPI-04-0899>.
- Srinivas, B., Sarin, M.M., Rengarajan, R., 2014. Atmospheric transport of mineral dust from the Indo-Gangetic Plain: temporal variability, acid processing, and iron solubility. *Geochem. Geophys. Geosyst.* 15, 3226–3243. <https://doi.org/10.1002/2014GC005395>.
- Stumm, W., Morgan, J.J., 2012. *Aquatic Chemistry: Chemical Equilibria and Rates in Natural Waters*. John Wiley & Sons.
- Sun, J., Shen, Z., Zhang, L., Lei, Y., Gong, X., Zhang, Q., Zhang, T., Xu, H., Cui, S., Wang, Q., Cao, J., Tao, J., Zhang, N., Zhang, R., 2019. Chemical source profiles of urban fugitive dust PM<sub>2.5</sub> samples from 21 cities across China. *Sci. Total Environ.* 649, 1045–1053.
- Tao, Y., Murphy, J.G., 2019. The mechanisms responsible for the interactions among oxalate, pH, and Fe dissolution in PM<sub>2.5</sub>. *ACS Earth Space Chem.* 3, 2259–2265. <https://doi.org/10.1021/acsearthspacechem.9b00172>.
- Tao, J., Zhang, L., Cao, J., Zhong, L., Chen, Dongsheng, Yang, Y., Chen, Duohong, Chen, L., Zhang, Z., Wu, Y., Xia, Y., Ye, S., Zhang, R., 2017. Source apportionment of PM<sub>2.5</sub> at urban and suburban areas of the Pearl River Delta region, south China – with emphasis on ship emissions. *Sci. Total Environ.* 574, 1559–1570. <https://doi.org/10.1016/j.scitotenv.2016.08.175>.
- Tao, J., Huang, J., Bian, G., Zhang, L., Zhou, Z., Zhang, Z., Li, J., Miao, Y., Yuan, Z., Sha, Q., Xiao, L., Wang, B., 2023. Fine particulate pollution driven by nitrate in the moisture urban atmospheric environment in the Pearl River Delta region of south China. *J. Environ. Manage.* 326, 116704 <https://doi.org/10.1016/j.jenman.2022.116704>.
- Thorpe, A., Harrison, R.M., 2008. Sources and properties of non-exhaust particulate matter from road traffic: a review. *Sci. Total Environ.* 400, 270–282. <https://doi.org/10.1016/j.scitotenv.2008.06.007>.
- Tian, H.Z., Lu, L., Hao, J.M., Gao, J.J., Cheng, K., Liu, K.Y., Qiu, P.P., Zhu, C.Y., 2013. A review of key hazardous trace elements in Chinese coals: abundance, occurrence, behavior during coal combustion and their environmental impacts. *Energy Fuel* 27, 601–614. <https://doi.org/10.1021/ef3017305>.
- Tyler, G., Olsson, T., 2001. Concentrations of 60 elements in the soil solution as related to the soil acidity. *Eur. J. Soil Sci.* 52, 151–165. <https://doi.org/10.1046/j.1365-2389.2001.t01-1-00360.x>.
- Verma, A., Kore, R., Corbin, D.R., Shiflett, M.B., 2019. Metal recovery using oxalate chemistry: a technical review. *Ind. Eng. Chem. Res.* 58, 15381–15393. <https://doi.org/10.1021/acs.iecr.9b02598>.
- Viana, M., Amato, F., Alastuey, A., Querol, X., Moreno, T., García Dos Santos, S., Herce, M.D., Fernández-Patier, R., 2009. Chemical tracers of particulate emissions from commercial shipping. *Environ. Sci. Technol.* 43, 7472–7477. <https://doi.org/10.1021/es901558t>.
- Wang, Q., Ma, Y., Tan, J., Zheng, N., Duan, J., Sun, Y., He, K., Zhang, Y., 2015. Characteristics of size-fractionated atmospheric metals and water-soluble metals in two typical episodes in Beijing. *Atmos. Environ.* 119, 294–303. <https://doi.org/10.1016/j.atmosenv.2015.08.061>.
- Wang, Z., Huang, X., Wang, N., Xu, J., Ding, A., 2020. Aerosol-radiation interactions of dust storm deteriorate particle and ozone pollution in East China. *J. Geophys. Res. Atmos.* 125, e2020JD033601 <https://doi.org/10.1029/2020JD033601>.
- Wang, G., Huang, K., Fu, Q., Chen, J., Huo, J., Zhao, Q., Duan, Y., Lin, Y., Yang, F., Zhang, W., Li, H., Xu, J., Qin, X., Zhao, N., Deng, C., 2022. Response of PM<sub>2.5</sub>-bound elemental species to emission variations and associated health risk assessment during the COVID-19 pandemic in a coastal megacity. *J. Environ. Sci.* 122, 115–127. <https://doi.org/10.1016/j.jes.2021.10.005>.
- Winton, V.H.L., Edwards, R., Bowie, A.R., Keywood, M., Williams, A.G., Chambers, S.D., Selleck, P.W., Desservet, M., Mallet, M.D., Paton-Walsh, C., 2016. Dry season aerosol iron solubility in tropical northern Australia. *Atmos. Chem. Phys.* 16, 12829–12848. <https://doi.org/10.5194/acp-16-12829-2016>.
- Wozniak, A.S., Shelley, R.U., Sleighter, R.L., Abdulla, H.A.N., Morton, P.L., Landing, W. M., Hatcher, P.G., 2013. Relationships among aerosol water soluble organic matter, iron and aluminum in European, North African, and marine air masses from the 2010 US GEOTRACES cruise. *Mar. Chem.* 154, 24–33. <https://doi.org/10.1016/j.marchem.2013.04.011>.
- Wu, Y., Li, G., Yang, Y., An, T., 2019. Pollution evaluation and health risk assessment of airborne toxic metals in both indoors and outdoors of the Pearl River Delta, China. *Environmental Research* 179, 108793. <https://doi.org/10.1016/j.envres.2019.108793>.
- Xu, M., Yan, R., Zheng, C., Qiao, Y., Han, J., Sheng, C., 2004. Status of trace element emission in a coal combustion process: a review. *Fuel Process. Technol.* 85, 215–237. [https://doi.org/10.1016/S0378-3820\(03\)00174-7](https://doi.org/10.1016/S0378-3820(03)00174-7).
- Yan, R.-H., Peng, X., Lin, W., He, L.-Y., Wei, F.-H., Tang, M.-X., Huang, X.-F., 2022. Trends and challenges regarding the source-specific health risk of PM<sub>2.5</sub>-bound metals in a Chinese megacity from 2014 to 2020. *Environ. Sci. Technol.* 56, 6996–7005. <https://doi.org/10.1021/acs.est.1c06948>.
- Yang, Y., Weber, R.J., 2022. Ultrafiltration to characterize PM<sub>2.5</sub> water-soluble iron and its sources in an urban environment. *Atmos. Environ.* 286, 119246 <https://doi.org/10.1016/j.atmosenv.2022.119246>.
- Yang, Y., Gao, D., Weber, R.J., 2021. A method for liquid spectrophotometric measurement of total and water-soluble iron and copper in ambient aerosols. *Atmos. Meas. Tech.* 14, 4707–4719. <https://doi.org/10.5194/amt-14-4707-2021>.
- Yu, G., Zhang, Y., Yang, F., He, B., Zhang, C., Zou, Z., Yang, X., Li, N., Chen, J., 2021. Dynamic Ni/V ratio in the ship-emitted particles driven by multiphase fuel oil

- regulations in coastal China. Environ. Sci. Technol. 55, 15031–15039. <https://doi.org/10.1021/acs.est.1c02612>.
- Zhang, R., Cao, J., Tang, Y., Arimoto, R., Shen, Z., Wu, F., Han, Y., Wang, G., Zhang, J., Li, G., 2014. Elemental profiles and signatures of fugitive dusts from Chinese deserts. Sci. Total Environ. 472, 1121–1129. <https://doi.org/10.1016/j.scitotenv.2013.11.011>.
- Zhang, H., Li, R., Dong, S., Wang, F., Zhu, Y., Meng, H., Huang, C., Ren, Y., Wang, Xinfeng, Hu, X., Li, T., Peng, C., Zhang, G., Xue, L., Wang, Xinning, Tang, M., 2022. Abundance and fractional solubility of aerosol iron during winter at a coastal city in Northern China: similarities and contrasts between fine and coarse particles. JGR Atmospheres 127. <https://doi.org/10.1029/2021JD036070>.
- Zhang, H., Li, R., Huang, C., Li, X., Dong, S., Wang, F., Li, T., Chen, Y., Zhang, G., Ren, Y., Chen, Q., Huang, R., Chen, S., Xue, T., Wang, X., Tang, M., 2023. Seasonal variation of aerosol iron solubility in coarse and fine particles at an inland city in northwestern China. Atmos. Chem. Phys. 23, 3543–3559. <https://doi.org/10.5194/acp-23-3543-2023>.
- Zhao, J., Zhang, Y., Xu, H., Tao, S., Wang, R., Yu, Q., Chen, Y., Zou, Z., Ma, W., 2021. Trace elements from ocean-going vessels in East Asia: vanadium and nickel emissions and their impacts on air quality. J. Geophys. Res. Atmos. 126, e2020JD033984 <https://doi.org/10.1029/2020JD033984>.
- Zhu, Y., Li, W., Lin, Q., Yuan, Q., Liu, L., Zhang, J., Zhang, Y., Shao, L., Niu, H., Yang, S., Shi, Z., 2020. Iron solubility in fine particles associated with secondary acidic aerosols in east China. Environ. Pollut. 264, 114769 <https://doi.org/10.1016/j.envpol.2020.114769>.
- Zhu, Y., Li, W., Wang, Y., Zhang, J., Liu, L., Xu, L., Xu, J., Shi, J., Shao, L., Fu, P., Zhang, D., Shi, Z., 2022. Sources and processes of iron aerosols in a megacity in Eastern China. Atmos. Chem. Phys. 22, 2191–2202. <https://doi.org/10.5194/acp-22-2191-2022>.